Synthesis of graphene-based nanosheets via chemical reduction of exfoliated graphite oxide

Sasha Stankovich [a], Dmitriy A. Dikin [a], Richard D. Piner [a], Kevin A. Kohlhaas [a],
Alfred Kleinhammes [c], Yuanyuan Jia [c], Yue Wu [c],
SonBinh T. Nguyen [b,*], Rodney S. Ruoff [a,*]

[a] *Department of Mechanical Engineering, Northwestern University, 2145 Sheridan Rd., Evanston, IL 60208-3133, USA*
[b] *Department of Chemistry, 2145 Sheridan Rd., Evanston, IL 60208-3113, USA*
[c] *Department of Physics and Astronomy and Curriculum in Applied and Materials Sciences, University of North Carolina, Chapel Hill, NC, 27599-3255, USA*

Abstract

Reduction of a colloidal suspension of exfoliated graphene oxide sheets in water with hydrazine hydrate results in their aggregation and subsequent formation of a high-surface-area carbon material which consists of thin graphene-based sheets. The reduced material was characterized by elemental analysis, thermo-gravimetric analysis, scanning electron microscopy, X-ray photoelectron spectroscopy, NMR spectroscopy, Raman spectroscopy, and by electrical conductivity measurements.
© 2007 Elsevier Ltd. All rights reserved.

1. Introduction

Graphite-like nanoplatelets have recently attracted attention as a viable and inexpensive filler in composite materials [1–3] that can be used in many engineering applications, given the excellent in-plane mechanical, structural, thermal, and electrical properties of graphite [4]. These excellent properties may be relevant at the nanoscale if graphite can be exfoliated into thin nanoplatelets, and even down to the single graphene sheet level [5].

Graphite nanoplatelets have often been made from expanded graphite, which in turn was produced from graphite intercalation compounds via rapid evaporation of the intercalant at elevated temperatures. For example, rapid thermal expansion of sulfuric acid-intercalated graphite, followed by a suitable treatment to produce plate-lets/nanoplatelets from the expanded material (ball milling or exposure to ultrasound) has been recently demonstrated [6–13]. Although this simple method has been applied on a large scale to commercially available sulfuric acid-intercalated graphite, it never results in complete exfoliation of graphite to the level of individual graphene sheets. The extent of thermal expansion (and therefore the platelet thickness) is dependent on the type of graphite used and on the intercalation procedure [14,15]. With few exceptions [3], the graphite nanoplatelets obtained via this process typically consist of hundreds of stacked graphene layers (assuming that the thickness of one layer is equal to the interlayer separation in graphite, 0.34 nm) and average between 30 and 100 nm in thickness.

In addition to the thermal expansion route, the delamination of intercalated graphite can sometimes be achieved by inducing a gas-producing chemical reaction within its interlayer galleries (chemical expansion). For example, a low-temperature chemical expansion route to graphite nanoplatelets and nanoscrolls, based on potassium-intercalated graphite, has been reported [16,17]. However, this approach could not be reproduced in our laboratory even

---

with a duplication of the expensive ultra-high-intensity ultrasonic equipment reported therein.

Given our interest in the preparation of graphene-based materials [18–20], we set out to develop a general and reproducible approach for the preparation of graphene sheets from graphite. After numerous failed attempts to create graphene-based sheets via graphite intercalation compounds, we decided to use graphite oxide (GO) as one possible route for meeting this challenge. Our basic strategy involved the complete exfoliation of GO into individual GO sheets followed by their *in-situ* reduction to produce individual graphene-like sheets [19,20]. Herein, we describe the detailed process for the reduction of exfoliated GO sheets with hydrazine and the characterization of the resulting material. In particular, we present evidence to support the claim that GO can be completely exfoliated into individual graphene oxide sheets and that chemical reduction of such sheets can furnish graphene-like sheets.

GO is produced by the oxidative treatment of graphite via one of three principal methods developed by Brodie [21], Hummers [22], and Staudenmeier [23], respectively. It still retains a layered structure, but is much lighter in color than graphite due to the loss of electronic conjugation brought about by the oxidation. According to the most recent studies [24–29], GO consists of oxidized graphene sheets (or 'graphene oxide sheets') having their basal planes decorated mostly with epoxide and hydroxyl groups, in addition to carbonyl and carboxyl groups located presumably at the edges (Lerf–Klinowski model). These oxygen functionalities render the graphene oxide layers of GO hydrophilic and water molecules can readily intercalate into the interlayer galleries. GO can therefore be also thought of as a graphite-type intercalation compound with both covalently bound oxygen and non-covalently bound water between the carbon layers. Indeed, rapid heating of GO results in its expansion and delamination caused by rapid evaporation of the intercalated water and evolution of gases produced by thermal pyrolysis of the oxygen-containing functional groups [30]. Such thermal treatment has recently been suggested to be capable of producing individual functionalized graphene sheets [30].

By nature, GO is electrically insulating (see below) and thus cannot be used, without further processing, as a conductive nanomaterial. In addition, the presence of the oxygen functional groups makes GO thermally unstable, as it undergoes pyrolysis at elevated temperatures [31,32]. Notably, it has been demonstrated that the electrical conductivity of GO (and presumably its thermal stability as well) can be restored close to the level of graphite by chemical reduction [33–36]. Such reductions of GO, however, have not been studied in great detail. To that end, we have examined the chemical reduction of exfoliated graphene oxide sheets with several reducing agents and found hydrazine hydrate ($H_2NNH_2 \cdot H_2O$) to be the best one in producing very thin graphene-like sheets, consistent with previous reports [31,32]. High-resolution scanning electron microscopy (SEM) also provided us with evidence of thin sheets. Here

we report a comprehensive study of this reduced material by elemental analysis, X-ray photoelectron spectroscopy (XPS), gas adsorption, solid state NMR spectroscopy, Raman spectroscopy, thermo-gravimetric analysis (TGA), SEM, and electrical conductivity measurements.

2. Experimental

2.1. Materials and methods

GO was prepared from purified natural graphite (SP-1, 30-μm nominal particle size, Bay Carbon, Bay City, MI) by the Hummers method [22]. SEM images were obtained with a field emission gun scanning electron microscope (LEO1525, Carl Zeiss SMT AG, Oberkochen, Germany). Samples for AFM imaging were prepared by depositing colloidal suspensions of GO on freshly cleaved mica surfaces (Ted Pella Inc., Redding, CA). AFM images were taken on a MultiTask AutoProbe CP/MT Scanning Probe Microscope (Veeco Instruments, Woodbury, NY). Imaging was done in non-contact mode using a V-shape "Ultralever" probe B (B-doped Si with frequency $f_c = 78.6$ kHz, spring constants $k = 2.0$–3.8 N/m, and nominal tip radius $r = 10$ nm, Park Scientific Instruments, Woodbury, NY). All images were collected under ambient conditions at 50% relative humidity and 23 °C with a scanning raster rate of 1 Hz.

Surface area analysis was performed with a Micromeritics ASAP 2010 Analyzer (Micromeritics Instrument Corporation, Norcross, GA). The samples were outgassed at 3 mTorr and 150 °C for 24 h prior to analysis. Elemental analyses and Karl–Fisher titration were performed by Galbraith Laboratories (Knoxville, TN). XPS measurements were performed using an Omicron ESCA Probe (Omicron Nanotechnology, Taunusstein, Germany) with a monochromated Al K$_\alpha$ radiation ($hv = 1486.6$ eV). TGA was performed under a nitrogen flow (100 mL/min) using a TA Instruments TGA-SDT 2960 on sample sizes from 5 to 6 mg, and the mass was recorded as a function of temperature. The samples were heated from room temperature to 800 °C at 5 °C/min. To avoid thermal expansion of the GO due to rapid heating, GO samples were also heated from room temperature to 800 °C at 1 °C/min.

Solid-state FT-NMR spectra were recorded on a Chemagnetic CMX 400 instrument equipped with a 4-mm magic angle spinning (MAS) probe at a magnetic field of 9.4 T. The neat samples (28 mg each) were spun at 9.4 kHz to average the anisotropic chemical shift tensor. Spectra based on free induction decays with moderate decoupling power were averaged over 18,000 scans with a recycle delay of 8s. The 90° pulse is 2.5 μs as determined by acquisition on adamantane. Solid adamantane (38.3 ppm) was also used as the external reference for ^{13}C chemical shift based on the TMS scale. Raman spectra were recorded from 200 to 2000 cm^{-1} on a Renishaw 2000 Confocal Raman Microprobe (Rhenishaw Instruments, England) using a 514.5-nm argon ion laser.

2.2. Reduction of exfoliated GO with hydrazine hydrate

In a typical procedure, GO (100 mg) was loaded in a 250-mL round-bottom flask and water (100 mL) was then added, yielding an inhomogeneous yellow-brown dispersion. This dispersion was sonicated using a Fisher Scientific FS60 ultrasonic bath cleaner (150 W) until it became clear with no visible particulate matter. Hydrazine hydrate (1.00 mL, 32.1 mmol) was then added and the solution heated in an oil bath at 100 °C under a water-cooled condenser for 24 h over which the reduced GO gradually precipitated out as a black solid. This product was isolated by filtration over a medium fritted glass funnel, washed copiously with water (5×100 mL) and methanol (5×100 mL), and dried on the funnel under a continuous air flow through the solid product cake.

2.3. Sample preparation and measurement of electrical conductivity

The electrical conductivity of the graphitic powders was measured at different apparent densities (created by compressing the samples to varying

degrees) by a method similar to that described in the literature [37]. Briefly, a given quantity of powder was poured into a glass tube (ID = 5 mm) and manually compressed between two copper plungers that fit closely to the tube ID. A DC power supply (Agilent 6613C, Agilent Technologies, Santa Clara, CA), picoampere meter (Keithley 6485, Keithley Instruments, Cleveland, OH), and multimeter (HP 34401A, Hewlett–Packard, CA) were connected to measure DC conductivity by a two-probe method. A digital micrometer (Mitutoyo Corporation, Kanagawa, Japan) was used to measure the height of the powder column at each compression step.

In the present work, values for electrical conductivity for pristine graphite, GO, and reduced GO, were determined by fitting the experimental data to the equation: $\sigma_c = \sigma_h [(\phi - \phi_c)/(1 - \phi_c)]^k$, derived from the general effective media (GEM) equation [38,39] with an assumption that the conductivity of the low-conductive phase (air) is zero. In this expression σ_c is the conductivity of the composite medium, σ_h and ϕ are the conductivity of the highly-conductive phase and their volume fraction, respectively, ϕ_c is the percolation threshold, and k is a critical exponent related to the percolation threshold and to the shape of the particles. This formula has identical form as in the geometrical percolation model (GPM) [40], with the exception of the critical exponent, k, which may have values different from the universal value of 2 as determined for the 3-dimensional GPM.

The two fitting parameters in the GEM equation are σ_h and k. The percolation threshold, ϕ_c, is determined as a ratio of the apparent powder density before compression, d_p, and the apparent density of the particles, d_g. The bulk density of graphite (2200 kg/m^3) has been used in all cases as a value for d_g. This assumption has been proven to be correct within an accuracy of 5% by measuring the apparent density of powder samples that were compressed at a pressure of 300 MPa.

3. Results and discussion

3.1. Exfoliation of GO in water

An important property of GO, brought about by the hydrophilic nature of the oxygenated graphene layers, is its easy exfoliation in aqueous media. As a result, GO readily forms stable colloidal suspensions of thin sheets in water [41,42]. After a suitable ultrasonic treatment, such exfoliation can produce stable dispersions of very thin graphene oxide sheets in water [18,19] These sheets are, however, different from graphitic nanoplatelets or pristine graphene sheets due to their low electrical conductivity.

In our work, sufficiently dilute colloidal suspensions of GO prepared with the aid of ultrasound are clear, homogenous, and stable indefinitely [18]. AFM images of GO exfoliated by the ultrasonic treatment at concentrations of 1 mg/mL in water always revealed the presence of sheets with uniform thickness (∼1 nm; an example is shown in Fig. 1). These well-exfoliated samples of GO contained no sheets either thicker or thinner than 1 nm, leading to a conclusion that complete exfoliation of GO down to individual graphene oxide sheets was indeed achieved under these conditions. While a pristine graphene sheet is atomically flat with a well-known van der Waals thickness of ∼0.34 nm, graphene oxide sheets are expected to be 'thicker' due to the presence of covalently bound oxygen and the displacement of the sp^3-hybridized carbon atoms slightly above and below the original graphene plane. From XRD experiments, the intersheet distance for GO varies with the amount of absorbed water, with values such as 0.63 nm and 0.61 nm reported for "dry" GO samples (complete drying of GO is probably impossible [28]) to 1.2 nm for hydrated GO [43]. If these values could be regarded as the "thickness" of a hydrated individual GO layer, given the uniformity of the observed thicknesses in our GO materials and that sheets one-half (or any other inverse integer value, such as one third, etc.) of the minimum thickness obtained by AFM are never observed, the GO sheets observed by AFM represent fully exfoliated graphene oxide sheets. (We note that heights significantly smaller than 1 nm are observable in our AFM experiment; an example of which is the observation of C_{12} amine adsorbed onto freshly cleaved mica from the vapor phase. This makes the mica hydrophobic in just a few minutes and when a new clean AFM tip is brought into contact with the monolayer, some of the C_{12} amine wicks up the tip and depletes the monolayer. The resulting voids left in the film are around 0.2 nm deep. Thus, if platelets with thicknesses that are less than those observed for the GO sheet samples discussed herein were present, they would be readily detected.)

3.2. Reduction of exfoliated GO

During the hydrazine reduction of graphene oxide sheets dispersed in water, the brown-colored dispersion turns
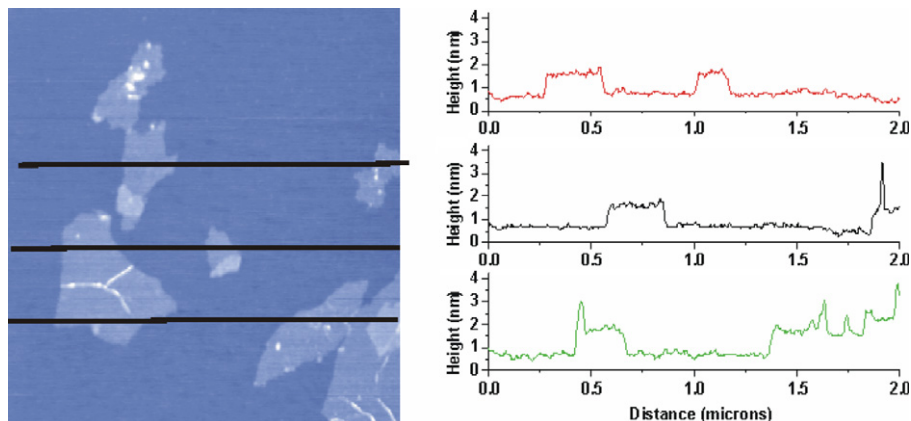
Fig. 1. A non-contact mode AFM image of exfoliated GO sheets with three height profiles acquired in different locations.

black and the reduced sheets aggregate and eventually pre-cipitate [18]. The precipitation of the reduced sheets occurs, presumably due to their becoming less hydrophilic as a result of oxygen removal (see discussion of elemental analysis, NMR, and XPS below) and thus increased incompatibility with the aqueous medium. As solvation of the reduced sheets decreases, the intersheet hydrophobic interactions cause them to aggregate as well as adhere to the hydrophobic surface of the Teflon-coated stir bar. All of our attempts to redisperse them in water or obtain stable dispersions of the reduced sheets in a number of organic solvents (dimethylformamide, tetrahydrofuran, toluene, chloroform, or chlorobenzene) failed.

3.3. Characterization of reduced GO

SEM images revealed that the reduced GO material consists of randomly aggregated, thin, crumpled sheets closely associated with each other and forming a disordered solid (Fig. 2a). The folded regions of the sheets (Fig. 2b) were found to have average widths of ~2 nm by high-resolution SEM. At the resolution limit of our instrument (see caption of Fig. 2), these data again suggest, but do not prove, the presence of individual sheets in our reduced GO materials. The absence of charging during the SEM imaging indicates that the network of graphene-based sheets and the individual sheets are electrically conductive. This qualitative conclusion was further confirmed by DC electrical measurements (see below).

Surface area measurement of the reduced GO sheets via nitrogen gas absorption yielded a BET value of 466 m^2/g (Fig. 3). This high specific surface area is partially an indication of the degree of GO exfoliation prior to the reduction. However, it is still lower than the theoretical specific surface area for completely exfoliated and isolated graphene sheets (~2,620 m^2/g [20]), potentially due to the agglomeration of the graphene oxide sheets upon reduction. While this agglomeration can result in the partial overlapping and coalescing of the reduced sheets and lowers the surface area of the bulk materials, the crumpled
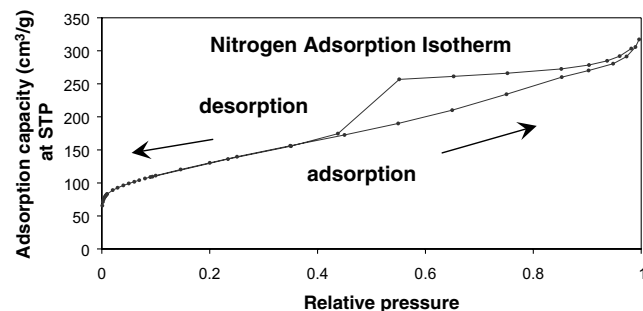
Fig. 3. Nitrogen adsorption and desorption isotherms for reduced exfoliated GO. The shape of the isotherm indicates that the material contains both micro and mesopores [53].

3-dimensional structure of the sheets (see above) still leaves many exposed surfaces.

Elemental analyses, coupled with Karl-Fisher titration, show an increase in C/O atomic ratio in the reduced material (10.3) compared to the starting GO (2.7) [18]. Karl-Fisher analysis was performed as GO is a hygroscopic material and any water that might be trapped between (or on) its layers would contribute to a higher oxygen content (water content as high as 25 wt% has been measured in our GO samples). The reduced GO has a much lower water content (2.8 wt%), consistent with its hydrophobic nature. Hence, it can be described as consisting of partially oxidized graphene nanoplatelets, given that some oxygen is still retained after reduction. The black color of the reduced GO materials also suggests a partial 're-graphitization' of the exfoliated GO. In addition to the decrease in the oxygen level, the reduction of GO is accompanied by some nitrogen incorporation from the reducing agent (C/N = 16.1 by elemental analysis), presumably through a reaction of hydrazine with the carbonyl groups of GO (see below) [18].

Although GO is thermally unstable and starts to lose mass upon heating even below 100 °C, the major mass loss occurs at ~200 °C, presumably due to pyrolysis of the labile oxygen-containing functional groups, yielding CO, CO_2, and steam [27,44]. Hence, the thermal decomposition
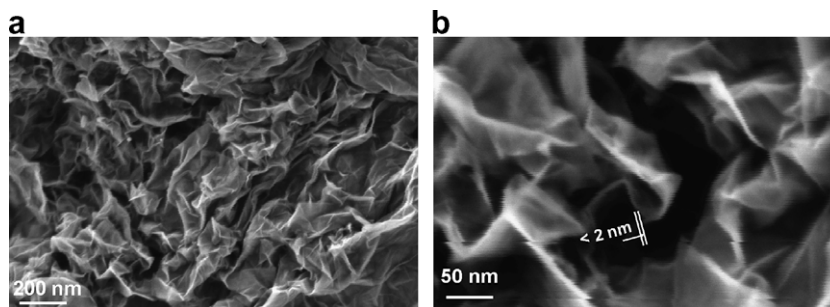
Fig. 2. (a) An SEM image of aggregated reduced GO sheets. (b) A platelet having an upper bound thickness at a fold of ~2 nm. At the resolution limit of the FEG SEM used here, the following are relevant parameters of the microscope and of the specimen. *Of the microscope*: spot size and flux of e-beam (e-current, density, solid angle/aperture size), energy of the electrons in the primary beam, electromagnetic lens alignment, type of detectors used and their operating parameters. *Of the sample*: geometry (such as edges, roughness, thickness, and orientation with respect to e-beam), material (such as density, atomic number, electrical conductivity, and composition), substrate or matrix (what the specimen is affixed to or a part of). There is also the role of the *operator expertise*. Thus for (b) and discussion of a measured value for the fold thickness of about 2 nm, we suggest a confidence limit of roughly ±1 nm.

of GO can be accompanied by a vigorous release of gas, resulting in a rapid thermal expansion of the material. This is evident by both a large volume expansion and a larger mass loss (from flying GO debris in the TGA instrument) during a more rapid heating regime (Fig. 4). On the other hand, the removal of the thermally labile oxygen functional groups by chemical reduction results in much increased thermal stability for the reduced GO. Apart from a slight mass loss below 100 °C, which can be attributed to the loss of adsorbed water, no significant mass loss is detected when this material is heated up to 800 °C.

The ^{13}C MAS NMR spectra of GO and the reduced GO indicate significant structural change induced by the reduction. In the spectrum of GO (Fig. 5), the peaks at 57 and 68 ppm represent the ^{13}C nuclei in the epoxide and hydroxyl groups, respectively [24–27]. The resonance at 130 ppm belongs to the un-oxidized sp^2 carbons of the graphene network and that at 188 ppm presumably arises from the carbonyl groups. In the ^{13}C spectrum of the reduced GO, the peaks from the oxygenated and the carbonyl carbons are absent. The remaining prominent feature is the resonance at 117 ppm that is broadened by chemical shift distribution and corresponds to variations of carbon atom environments.
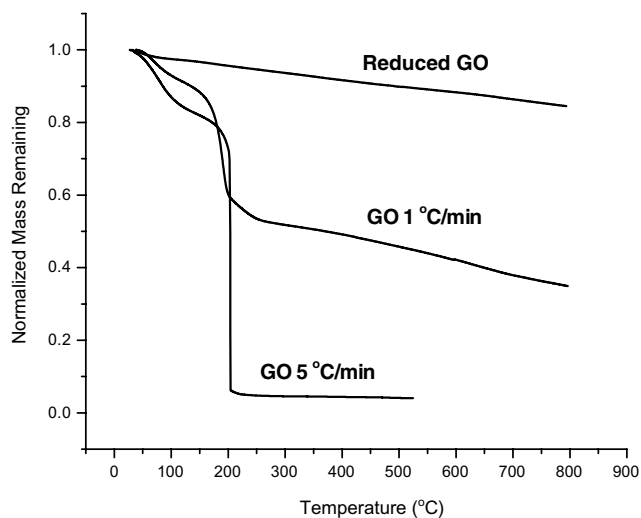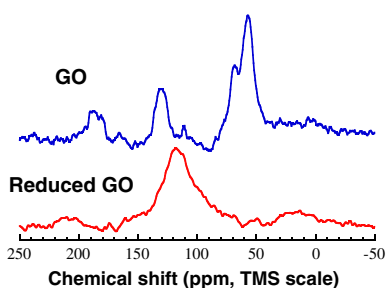
Previously, we have employed XPS to analyze GO and the reduced exfoliated GO [18]. In brief, the C1s XPS spectrum of GO (Fig. 6a) clearly indicates a considerable degree of oxidation with four components that correspond to carbon atoms in different functional groups: the non-oxygenated ring C, the C in C–O bonds, the carbonyl C, and the carboxylate carbon (O–C=O) [45,46]. Although the C1s XPS spectrum of the reduced exfoliated GO (Fig. 6b) also exhibits these same oxygen functionalities, their peak intensities are much smaller than those in GO. In addition, there is an additional component at 285.9 eV corresponding to C bound to nitrogen [46]. These observations are consistent with the elemental analysis data (see above) and again indicate both considerable de-oxygenation by the reduction process as well as nitrogen incorporation.

The significant structural changes occurring during the chemical processing from pristine graphite to GO, and then to the reduced GO, are also reflected in their Raman spectra (Fig. 7). The Raman spectrum of the pristine graphite, as expected, displays a prominent G peak as the only feature at 1581 cm^{-1}, corresponding to the first-order scattering of the E2g mode [47]. In the Raman spectrum of GO, the G band is broadened and shifted to 1594 cm^{-1}. In addition, the D band at 1363 cm^{-1} becomes prominent, indicating the reduction in size of the in-plane sp^2 domains, possibly due to the extensive oxidation. The Raman spectrum of the reduced GO also contains both G and D bands (at 1584 and 1352 cm^{-1}, respectively); however, with an increased D/G intensity ratio compared to that in GO. This change suggests a decrease in the average size of the sp^2 domains upon reduction of the exfoliated GO [47], and can be explained if new graphitic domains were created that are smaller in size to the ones present in GO before reduction, but more numerous in number.

Fig. 4. Normalized TGA plots for GO and the reduced GO. The downward slopes are due to normal instrument drift.

Fig. 5. Solid-state ^{13}C MAS NMR spectra of GO (top) and reduced exfoliated GO (bottom).
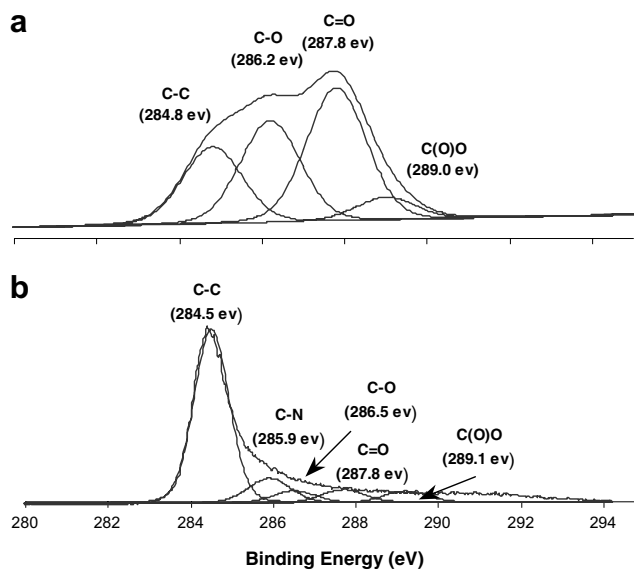
Fig. 6. The C1s XPS spectra of: (a) GO, (b) reduced GO. Adapted from reference [18].
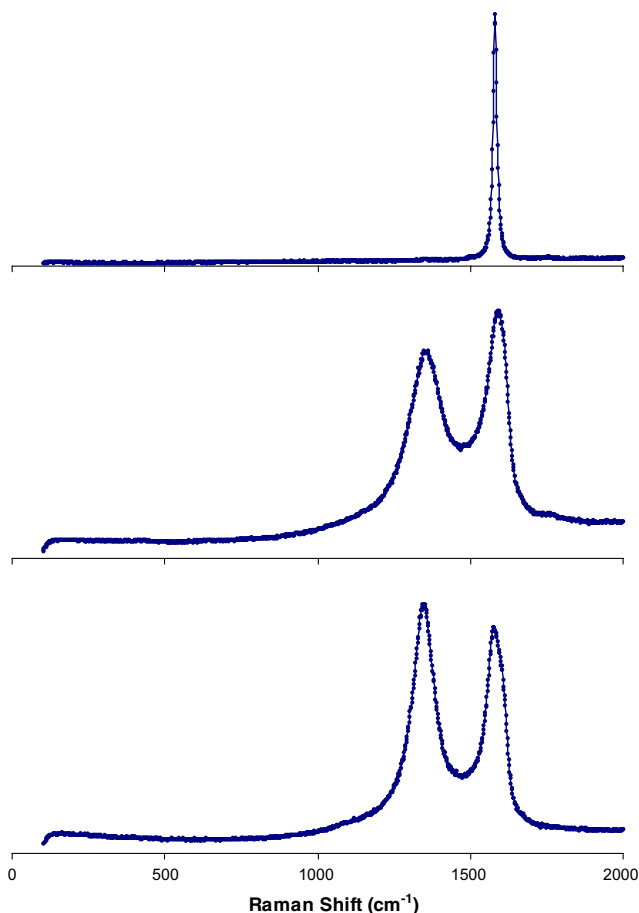
Fig. 7. The Raman spectra of SP-1 graphite (top), GO (middle), and the reduced GO (bottom).

Table 1
Fitting parameters describing percolation transport for the three graphitic powders shown in Fig. 8

	Pristine graphite (SP-1)	GO	Reduced GO
$\phi_c = d_p/d_g$	0.46	0.38	0.055
σ_h [S/m]	2500 ± 15	0.0206 ± 0.002	2420 ± 200
k	0.56 ± 0.03	1.6 ± 0.05	0.96 ± 0.02

To determine the extent to which the chemical reduction of exfoliated GO restores the electrical properties of the graphitic network, we measured the room-temperature electrical conductivities of compressed-powder samples of the pristine graphite, GO, and the reduced GO at 30% relative humidity (Fig. 8). The results of the fits to the experimental data are summarised in Table 1. The extrapolated intrinsic conductivity, σ_h, of the reduced GO is probably over-estimated due to the limited data range available as a result of the low compressibility and possible spatial variations in the density of the material. More reliable are the conductivity data for the reduced GO, which can be measured at higher powder compression. This conductivity ($\sim 2 \times 10^2$ S/m) is about 5 orders of magnitude better than the conductivity of GO, and closely approaches that of pristine graphite (approximately 10 times lower than the conductivity of pristine graphite powder at only about 10% of the bulk graphite density). Such high intrinsic conductivity of the reduced GO in spite of the presence of oxygen (potential acceptor sites) might be an indication of: (i) quite conductive particle-to-particle interfaces, which often determines the overall percolation conductivity; (ii) a very dense conductive network with many cross-linked connections; and (iii) possible ionic channels of charge transfer across the sample. This last mechanism is definitely a dominant one in the electrical conduction of GO powder and a reason for its high sensitivity to temperature and environmental humidity. In contrast, the conductivity of the reduced GO is based primarily on inter-particle contacts and is much less sensitive to environmental conditions.

We stress here that the aforementioned experimentally determined conductivities greatly depend on the measurement parameters, from the height and cross-sectional area of the sampled column and the applied pressure to the particle surface area and aspect ratio, environmental temperature, and humidity. The last two are especially important in measurements of GO conductivity due to its hydrophilic nature. It is therefore not straightforward to obtain an 'absolute value' of powder conductivity so that our results could be compared with others reported in the literature.

3.4. Possible mechanisms for the chemical reduction of GO by hydrazine

While results from both elemental analysis and XPS clearly show that reduction of the exfoliated GO results in considerable removal of oxygen (see above), our ^{13}C MAS NMR data additionally suggest that the reduction/de-oxygenation of GO also results in significant restoration of the sp^2 carbon sites. The same conclusion can be reached through the electrical conductivity measurements since the observed increase in conductivity upon reduction of GO requires that conductive pathways of conjugated carbon atoms be re-established. However, it is not chemically obvious how treatment of GO with hydrazine can lead to

Fig. 8. Conductivity as a function of the volume fraction of three different graphitic powders: pristine graphite (SP-1), GO, and reduced GO.

deoxygenation and the increase in unsaturation that accompanies re-graphitization (see below).

If the Lerf–Klinowski model (see above) is assumed to be correct, most of the oxygen functionalities in GO should be present in the form of either hydroxyl or epoxide groups [24–27]. Additionally, GO is believed to also contain a number of carbonyl-containing oxygen functionalities such as lactones, anhydrides, and quinones. The presence of these latter moieties can be used to explain the incorporation of nitrogen into the reduced GO, since hydrazine can react with anhydrides and lactones to form hydrazides and with quinones to form hydrazones [48]. However, only hydrazone formation results in the removal of oxygen. Further reduction of the hydrazone to yield a deoxygenated sp^2-carbon can also occur if it is situated adjacent to an epoxide (Wharton reaction) [49]. The possibility of a Wolff–Kishner-type reduction of the carbonyl groups seems unlikely given the low temperature and low basicity of the reaction media. Nevertheless, these three processes cannot account for all the removed oxygen during hydrazine reduction as carbonyl groups are not believed to be the dominant oxygen functionalities in GO. The key question, therefore, is how oxygen is removed from the epoxides and hydroxyls.

Hydrazine is known to readily ring-open epoxides and form hydrazino alcohols [50]. Though such a reaction pathway is possible in GO upon hydrazine treatment, it cannot be the dominant one since ring-opening of the epoxides with hydrazine in itself would not result in any oxygen removal. Further, the epoxides in GO are presumably quaternary and thus are not susceptible to a direct nucleophilic attack due to steric reasons. Finally, the modest extent of observed nitrogen incorporation also renders this pathway unlikely to be the only mode of epoxide reaction in GO. It is possible, however, that the initial derivative produced by the epoxide opening with hydrazine reacts further via the formation of an aminoaziridine moiety which would then undergo thermal elimination of diimide to form a double bond (Fig. 9) [51,52]. Such a reaction might be further driven in GO by re-establishment of the conjugated graphene network.

Ultimately, our analysis still leaves open the question of how, or even if, the hydroxyl oxygen is removed. The answer to this intriguing query constitutes a fertile research area that awaits further investigations by both experimenters and theorists. A theory that confirms the Lerf–Klinowski model of GO and lends support to the NMR-evaluated proportions of tetra-substituted epoxide moieties vs other oxygen-functionalities, before and after reduction, would be a significant advancement. In addition, thorough isotope-labeling studies, coupled to sophisticated *in-situ* spectroscopic experiments during the reduction, are necessary to deconvolute the chemical pathways of GO reduction.
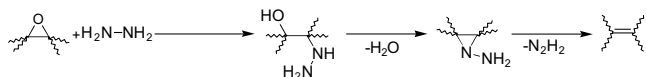
4. Conclusion

In conclusion, reduction of exfoliated graphene oxide sheets in water with hydrazine results in a material with graphitic characteristics that are comparable to those of pristine graphite. On the nanoscale, this carbon-based material consists of thin graphene-based sheets and possesses a high specific surface area. The characterization of the reduced GO indicates that the hydrazine treatment results in the formation of unsaturated and conjugated carbon atoms, which in turn imparts electrical conductivity. As such, reduced graphene oxide sheets may find use in a variety of applications such as hydrogen storage and as an electrically conductive filler material in composites.

References

[1] Drzal LT, Fukushima H. Graphite nanoplatelets as reinforcements for polymers. Polym Prepr (Am Chem Soc, Div Polym Chem) 2001;42(2):42–3.
[2] Drzal LT, Fukushima H. Exfoliated graphite as a nano-reinforcement for polymers. Int SAMPE Symp Ex 2003:1635–42.
[3] Fukushima H, Drzal LT. A carbon nanotube alternative: Graphite nanoplatelets as reinforcements for polymers. Ann Tech Conf – Soc Plast Eng 2003:2230–4.
[4] Kelly BT. Physics of graphite. London: Applied Science; 1981.
[5] Kotov NA. Materials science: Carbon sheet solutions. Nature 2006;442(7100):254–5.
[6] Chen G, Wu D, Weng W, Yan W. Dispersion of graphite nanosheets in a polymer matrix and the conducting property of the nanocomposites. Polym Eng Sci 2001;41(12):2148–54.
[7] Chen G, Wu D, Weng W, Wu C. Exfoliation of graphite flake and its nanocomposites. Carbon 2003;41(3):619–21.
[8] Chen G, Weng W, Wu D, Wu C. PMMA/graphite nanosheets composite and its conducting properties. Eur Polym J 2003;39(12):2329–35.
[9] Chen G, Wu C, Weng W, Wu D, Yan W. Preparation of polystyrene/graphite nanosheet composite. Polymer 2003;44(6):1781–4.
[10] Chen G, Weng W, Wu D, Wu C, Lu J, Wang P, et al. Preparation and characterization of graphite nanosheets from ultrasonic powdering technique. Carbon 2004;42(4):753–9.
[11] Kwon O, Choi S, Park K, Kwon Y. The preparation of exfoliated graphite by using microwave. J Ind Eng Chem (Seoul, Repub Korea) 2003;9(6):743–7.
[12] Weng W-G, Chen G-H, Wu D-J, Yan W-L. HDPE/expanded graphite electrically conducting composite. Compos Interf 2004;11(2):131–43.
[13] Weng W, Chen G, Wu D, Chen X, Lu J, Wang P. Fabrication and characterization of nylon 6/foliated graphite electrically conducting

Fig. 9. A proposed reaction pathway for epoxide reduction with hydrazine.

nanocomposite. J Polym Sci, Part B: Polym Phys 2004;42(15): 2844–56.

[14] Chung DDL. Exfoliation of graphite. J Mater Sci 1987;22(12): 4190–98.

[15] Chung DDL. Review graphite. J Mater Sci 2002;37(8):1475–89.

[16] Viculis LM, Mack JJ, Kaner RB. A chemical route to carbon nanoscrolls. Science 2003;299(5611):1361.

[17] Viculis LM, Mack JJ, Mayer OM, Hahn HT, Kaner RB. Intercalation and exfoliation routes to graphite nanoplatelets. J Mater Chem 2005;15(9):974–8.

[18] Stankovich S, Piner RD, Chen X, Wu N, Nguyen ST, Ruoff RS. Stable aqueous dispersions of graphitic nanoplatelets via the reduction of exfoliated graphite oxide in the presence of poly(sodium 4-styrenesulfonate). J Mater Chem 2006;16(2):155–8.

[19] Stankovich S, Piner RD, Nguyen ST, Ruoff RS. Synthesis and exfoliation of isocyanate-treated graphene oxide nanoplatelets. Carbon 2006;44(15):3342–7.

[20] Stankovich S, Dikin DA, Dommett GHB, Kohlhaas KM, Zimney EJ, Stach EA, et al. Graphene-based composite materials. Nature 2006;442(7100):282–6.

[21] Brodie BC. Sur le poids atomique du graphite. Ann Chim Phys 1860;59:466–72.

[22] Hummers W, Offeman R. Preparation of graphitic oxide. J Am Chem Soc 1958;80:1339.

[23] Staudenmaier L. Verfahren zur darstellung der graphitsaure. Ber Dtsch Chem Ges 1898;31:1481–99.

[24] He H, Riedl T, Lerf A, Klinowski J. Solid-state NMR studies of the structure of graphite oxide. J Phys Chem 1996;100(51):19954–8.

[25] He H, Klinowski J, Forster M, Lerf A. A new structural model for graphite oxide. Chem Phys Lett 1998;287(1,2):53–6.

[26] Lerf A, He H, Riedl T, Forster M, Klinowski J. ^{13}C and ^{1}H MAS NMR studies of graphite oxide and its chemically modified derivatives. Solid State Ionics 1997;101–103(Pt. 2):857–62.

[27] Lerf A, He H, Forster M, Klinowski J. Structure of graphite oxide revisited. J Phys Chem B 1998;102(23):4477–82.

[28] Szabo T, Berkesi O, Dekany I. DRIFT study of deuterium-exchanged graphite oxide. Carbon 2005;43(15):3186–9.

[29] Hontoria-Lucas C, Lopez-Peinado AJ, Lopez-Gonzalez JdD, Rojas-Cervantes ML, Martin-Aranda RM. Study of oxygen-containing groups in a series of graphite oxides: Physical and chemical characterization. Carbon 1995;33(11):1585–92.

[30] Schniepp HC, Li J-L, McAllister MJ, Sai H, Herrera-Alonso M, Adamson DH, et al. Functionalized single graphene sheets derived from splitting graphite oxide. J Phys Chem B 2006;110(17):8535–9.

[31] Boehm HP, Clauss A, Fischer GO, Hofmann U. Thin carbon leaves. Z Naturforsch 1962;17b:150–3.

[32] Boehm HP, Clauss A, Fischer GO, Hofmann U. The adsorption behavior of very thin carbon films. Z Anorg Allg Chem 1962;316:119–27.

[33] Bourlinos AB, Gournis D, Petridis D, Szabo T, Szeri A, Dekany I. Graphite oxide: Chemical reduction to graphite and surface modification with primary aliphatic amines and amino acids. Langmuir 2003;19(15):6050–5.

[34] Hofmann U, Frenzel A. The reduction of graphite oxide by hydrogen sulfide. Kolloid-Z 1934;68:149–51.

[35] Xiao P, Xiao M, Liu P, Gong K. Direct synthesis of a polyaniline-intercalated graphite oxide nanocomposite. Carbon 2000;38(4):626–8.

[36] Kotov NA, Dekany I, Fendler JH. Ultrathin graphite oxide-polyelectrolyte composites prepared by self-assembly. Transition between conductive and non-conductive states. Adv Mater 1996;8(8):637–41.

[37] Celzard A. Electrical conductivity of carbonaceous powders. Carbon 2002;40:2801–15.

[38] McLachlan DS. Equations for the conductivity of macroscopic mixtures. J Phys C: Solid State Phys 1986;19(9):1339–54.

[39] McLachlan DS. An equation for the conductivity of binary mixtures with anisotropic grain structures. J Phys C: Solid State Phys 1987;20(7):865–77.

[40] Kirkpatrick S. Percolation and conduction. Rev Mod Phys 1973;45:574–88.

[41] Titelman GI, Gelman V, Bron S, Khalfin RL, Cohen Y, Bianco-Peled H. Characteristics and microstructure of aqueous colloidal dispersions of graphite oxide. Carbon 2005;43(3):641–9.

[42] Szabo T, Tombacz E, Illes E, Dekany I. Enhanced acidity and ph-dependent surface charge characterization of successively oxidized graphite oxides. Carbon 2006;44(3):537–45.

[43] de Boer JH, van Doorn ABC. Graphite oxide. I. The adsorption of water. Koninkl Ned Akad Wetenschap, Proc 1958;61B:242–52.

[44] Wang G, Yang Z, Li X, Li C. Synthesis of poly(aniline-co-o-anisidine)-intercalated graphite oxide composite by delamination/reassembling method. Carbon 2005;43(12):2564–70.

[45] Briggs D, Beamson G. High resolution XPS of organic polymers: The scienta ESCA300 database. New York: John Wiley and Sons; 1992.

[46] Waltman RJ, Pacansky J, Bates Jr CW. X-ray photoelectron spectroscopic studies on organic photoconductors: Evaluation of atomic charges on chlorodiane blue and *p*-(diethylamino)benzaldehyde diphenylhydrazone. Chem Mater 1993;5(12):1799–804.

[47] Tuinstra F, Koenig JL. Raman spectrum of graphite. J Chem Phys 1970;53(3):1126–30.

[48] Neidlein R, Dao TV, Gieren A, Kokkinidis M, Wilckens R, Geserich HP, et al. Syntheses, structures, X-ray structure analyses, and electrical properties of di- and polychalcogen diimides. I. Chem Ber 1982;115(8):2898–904.

[49] Wharton PS, Bohlen DH. Hydrazine reduction of α,β-epoxy ketones to allylic alcohols. J Org Chem 1961;26:3615–6.

[50] Zalan Z, Lazar L, Fueloep F. Chemistry of hydrazinoalcohols and their heterocyclic derivatives. Part 1. Synthesis of hydrazinoalcohols. Curr Org Chem 2005;9(4):357–76.

[51] Mueller RK, Felix D, Schreiber J, Eschenmoser A. Stereochemistry of the thermal fragmentation of substituted *n*-aminoaziridine hydrazones. Helv Chim Acta 1970;53(6):1479–84.

[52] Lahti PM. Aziridinamine chemistry. I. Thermal decomposition of cis- and trans-2,3-diphenylaziridinamine. Tetrahedron Lett 1983;24(23):2339–42.

[53] Webb PA, Orr K. Analytical methods in fine particle technology. Norcross, GA: Micromeritics Instrument Corporation; 1997.